EPR imaging characterization of natural and synthetic materials

Timophey V. Popov

May 31, 2006

Abstract

In this paper one more kind of Magnetic Resonance Imaging will be discussed – Electron Paramagnetic Resonance Imaging (EPRI). It based on EPR phenomenon and uses the usual mathematical concepts of data obtaining typical for almost any sort of tomography – Radon transformation. Further material describes the way of gathering experimental information step-by-step from the very begining (theory and practice) to the high-end applications.

Contents

1 Introduction

Tomography is imaging by sections or sectioning. A device used in tomography is called a tomography, while the image produced is a tomogram. The method is used in medicine, archaeology, biology, geology, materials science and other sciences. It is based on the mathematical procedure called tomographic reconstruction. There are many different types of tomography, as listed below [3].

Atom probe tomography (APT) The atom probe is an atomic-resolution microscope used in materials science that was invented in 1967 by Erwin M?ller. APT uses a position-sensitive detector to deduce the lateral location of atoms. It was invented in 1988 by Alfred Cerezo, Terence Godfrey, and George D. W. Smith.

Computed tomography (CT) CT, originally known as computed axial tomography (CAT or CAT scan) and body section roentgenography, is a medical imaging method employing tomography where digital geometry processing is used to generate a three-dimensional image of the internals of an object from a large series of two-dimensional X-ray images taken around a single axis of rotation. CT produces a volume of data which can be manipulated, through a process known as windowing, in order to demonstrate various structures based on their ability to block the x-ray beam.

Confocal laser scanning microscopy (LSCM) CLSM or LSCM is a valuable tool for obtaining high resolution images and 3-D reconstructions. The key feature of confocal microscopy is its ability to produce blur-free images of thick specimens at various depths. Images are taken point-by-point and reconstructed with a computer, rather than projected through an eyepiece.

Cryo-electron tomography (Cryo-ET) Cryo-ET is a type of electron cryomicroscopy where tomography is used to obtain a 3D reconstruction of a sample is from tilted 2D images at cryogenic temperatures.

Electrical impedance tomography (EIT) EIT, is a medical imaging technique in which an image of the conductivity or permittivity of part of the body is inferred from surface electrical measurements. Typically conducting electrodes are attached to the skin of the subject and small alternating currents applied to some or all of the electrodes. The resulting electrical potentials are measured, and the process repeated for numerous different configurations of applied current. Proposed applications include monitoring of lung function, detection of cancer in the skin and breast and location of epileptic foci. All applications are currently considered experimental.

Magnetic resonance imaging (MRI) MRI, formerly referred to as magnetic resonance tomography (MRT) or nuclear magnetic resonance (NMR), is a method used to visualize the inside of living organisms as well as to detect the amount of bound water in geological structures. It is primarily used to demonstrate pathological or other physiological alterations of living tissues and is a commonly used form of medical imaging.

Functional magnetic resonance imaging (fMRI) fMRI is the use of MRI to measure the haemodynamic response related to neural activity in the brain or spinal cord of humans or other animals. It is one of the most recently developed forms of neuroimaging.

Optical coherence tomography (OCT) OCT is an interferometric, non-invasive optical tomographic imaging technique offering millimeter penetration (approximately 2–3 mm in tissue) with sub-micrometre axial and lateral resolution. By now OCT has found its place as a widely accepted imaging technique, especially in ophthalmology and other biomedical applications.

Positron emission tomography (PET) PET is a nuclear medicine medical imaging technique which produces a three dimensional image or map of functional processes in the

body. A short-lived radioactive tracer isotope which decays by emitting a positron, chemically incorporated into a metabolically active molecule, is injected into the living subject (usually into blood circulation). There is a waiting period while the metabolically active molecule (usually a sugar) becomes concentrated in tissues of interest, then the subject is placed in the imaging scanner. The short-lived isotope decays, emitting a positron. After travelling up to a few millimeters the positron annihilates with an electron, producing a pair of annihilation photons (similar to gamma rays) moving in opposite directions. These are detected when they reach a scintillator material in the scanning device, creating a burst of light which is detected by photomultiplier tubes. The technique depends on simultaneous or coincident detection of the pair of photons: photons which do not arrive in pairs (i.e., within a few nanoseconds) are ignored.

Quantum tomography Quantum tomography or quantum state tomography is the process of reconstructing the quantum state (density matrix) for a source of quantum systems by measurements on the systems coming from the source. To be able to uniquely identify the state, the measurements must be tomographically complete, that is the measured operators must form an operator basis on the Hilbert space of the system.

Single photon emission computed tomography (SPECT) SPECT is a nuclear medicine tomographic imaging technique using gamma rays. It is very similar to conventional nuclear medicine planar imaging using a gamma camera. However, it is able to provide true 3D information. This information is typically presented as cross-sectional slices through the patient, but can be freely reformatted or manipulated as required.

Seismic tomography Seismic tomography uses digital seismographic records to image the interior of the Earth.The basic scheme is to first localize and characterize a set of significant earthquakes. These earthquakes are then considered to "illuminate" the interior of the earth with seismic waves.The time that the waves arrive at seismic stations can then be used to calculate the waves' speed through the Earth. By combining analyses from many earthquakes, in different places around the Earth, a three dimensional map of wave speed through the Earth can be constructed.

X-ray Tomography X-ray Tomography is a branch of X-ray microscopy. A series of projection images are used to calculate a 3-Dimensional reconstruction of an object. The technique has found many applications in materials science and, lately, in biology and biomedicine.

In this paper one more kind of Magnetic Resonance Imaging will be discussed – Electron Paramagnetic Resonance Imaging (EPRI). It based on EPR phenomenon and uses the usual mathematical concepts of data obtaining typical for almost any sort of tomography – Radon transformation. Further material describes the way of gathering experimental information step-by-step from the very begining (theory and practice) to the high-end applications.

2 Introduction to Electron Paramagnetic Resonance phenomenon

EPR has matured into a powerful, versatile, non-destructive and noninstrusive analytical method. Unlike many other analytical techniques, EPR can produce meaningful structural and dynamical information, even from ongoing chemical and/or physical processes without influencing the process itself. Therefore, EPR is an ideal complementary technique for other methods in a wide of range of studies in the area of Chemistry, Biology, Medicine and Physics. The typical applications in each area can be outlined as followings [2].

2.1 EPR spectroscopy

In the early part of this century, scientists found that a molecule or atom has discrete (or separate) states, each with a corresponding energy. Spectroscopy is the measurement and interpretation of the differences in these energies. With this information, you gain insight into the identity, structure, and dynamics of the samples under study.

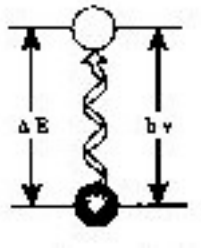

Figure 1: Transition associated with the absorption of electromagnetic energy.

The energy differences, ΔE ,can be measured, because of an important relationship between ΔE and the absorption of electromagnetic radiation. According to Planck's law, electromagnetic radiation may be absorbed if

$$\Delta E = h\nu \tag{1}$$

where h is Planck's constant and ν is the frequency of the radiation. The absorption of energy causes a transition from the lower energy to the higher energy state. The frequency at which the absorption occurs correspond to the energy differences of the states. Typically, the frequencies vary from Megahertz, through visible light, to ultraviolet light. Radiation in the Gigahertz range is used for EPR experiments.

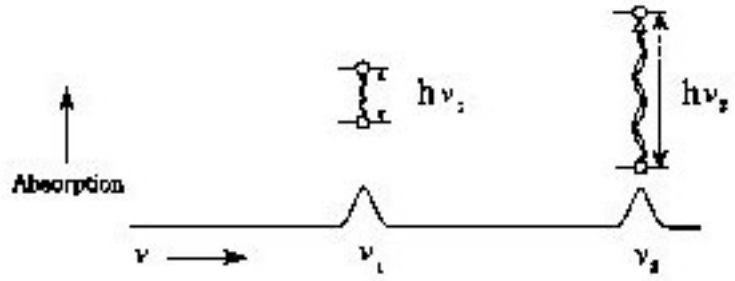

Figure 2: A spectrum.

The energy differences we study in EPR spectroscopy are due to the interaction of unpaired electrons in the sample with an external magnetic field produced by the EPR spectrometer. This effect is called Zeeman Effect.

Because the electron has a magnetic moment, it acts like a compass when you place it in a magnetic field, B_0. It will have a state of lowest energy when the moment of electron, μ is aligned along the magnetic field and a state with highest energy when μ is aligned against the magnetic field. The two states are labelled by the projection of electron spin, M_s, on the direction of the magnetic field. Because the electron is a spin 1/2 particle, the parallel state is designed as M_s= -1/2 and the antiparallel state is M_s = + 1/2. From quantum mechanics, we obtained the most basic equations of EPR

$$E = \mathbf{g}\ \mu_B B_0 M_s = \pm 1/2 g \mu_B B_0 \tag{2}$$

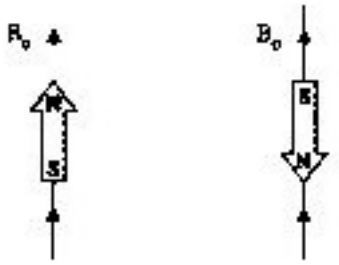

Figure 3: Minimum and maximum energy orientation of μ with respect to the magnetic field.

and

$$\Delta E = h\nu = g\mu_B B_0 \tag{3}$$

g is the g-factor, which is a proportionality constant approximately equal to 2 for most samples, but varies depending on the electronic configuration of the radical or ion. μB is the electron Bohr magneton, which is the natural unit of electronic magnetic moment.

For a single electron

- The two spin states have the same energy in the absence of a magnetic field.
- The energies of spin states diverge linearly as the magnetic field increases.

Therefore,

- Without a magnetic field, there is no energy difference to measure.
- The measured energy difference depends linearly on the magnetic field.

Because we can change the energy differences between the two spin states by varying the magnetic field strength, we have an alternative means to obtain spectra. We could apply a constant magnetic field and scan the frequency of the electromagnetic radiation as in conventional spectroscopy. Alternatively, we could keep the electromagnetic radiation frequency constant and scan the magnetic field. A peak in the absorption will occur when the magnetic field "tunes" the two spin states so that their energy difference matches the energy of the radiation. This field is called the "field for resonance". Owing to the limitations of microwave generators, the latter method offers superior performance, therefore, EPR spectrometers use this technique. Note for instrumental reasons a first derivative of the absorption is usually recorded.

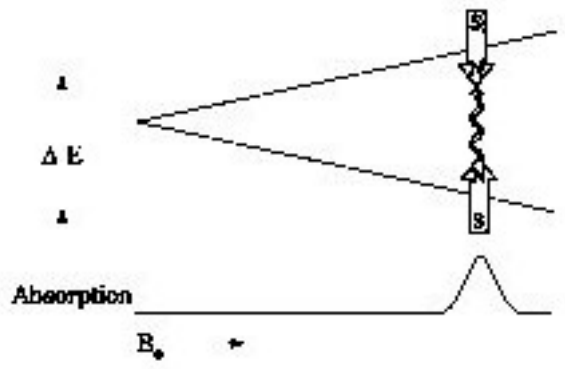

Figure 4: Variation of the spin state energies as a function of the applied magnetic field.

The field for resonance is not a unique fingerprint for identification of a compound because spectra can be acquired at several different frequencies. The g-factor

$$g = \frac{h\nu}{\mu_B B_0} \tag{4}$$

being independent of the microwave frequency, is much better for that purpose. The fields for resonance for a $g = 2$ signal at various microwave frequencies are given below.

Frequency (GHz)	Resonance field (T)
1.1	0.0393
3.5	01250
9.25	0.3305
24.0	0.8574
35.0	1.2504
90	3.2153
180	6.4305
270	9.6458

2.2 Hyperfine Interactions

Measurement of g-factors can give us some useful information, however, it does not tell us much about the molecular structure of the sample. Fortunately, the unpaired electron is very sensitive to its local surroundings. The nuclei of the atoms in a molecule or complex often have a magnetic moment, which produces a local magnetic field at the electron. The interaction between an unpaired electron and nuclei with non-zero nuclear spin is called the hyperfine interaction. It can give rise to features in an EPR spectrum. The interaction between the unpaired electron and the metal nuclear spin is termed the metal hyperfine interaction, whilst the corresponding interaction with a ligand nucleus is ligand hyperfine (or alternatively the superhyperfine) interaction. The metal hyperfine interaction will be represented by the symbol A, whilst that for a ligand atom, L by a_L. Any observed hyperfine coupling constant theoretically consists of two contributions; *isotropic and anisotropic*. The isotropic (or Fermi contact) contribution A_{iso} (or a_{iso} for ligands), is a measurement of the s orbital character of the unpaired electron. Anisotropic contributions depend upon the orbital angular momentum of the electron and hence are measure of d and/or p orbital character. The observed hyperfine interaction contains both isotropic and anisotropic contributions. For strictly octahedral, tetrahedral or cubic complexes the hyperfine interaction is isotropic. In general anisotropic contributions average to zero. Because of this when an anisotropic paramagnet is tumbling much more rapidly than the time-scale of the EPR experiment only the isotropic contribution is observed.

2.3 Isotropic paramagnets

The major effect in the EPR spectrum of electron spin-nuclear spin interaction can be illustrated by considering an "isolated atom" with one unpaired electron $S = 1/2$, and a nucleus with a nuclear spin of one half ($I = 1/2$). Each energy state of the electron in the magnetic field can be split symmetrically into two components (Figure 5, solid lines). The EPR spectrum is controlled by the selection rule $\Delta m_s = \pm 1$, $\Delta m_I = 0$, which results in two resonances of equal intensity (Figure 6). These resonances are displaced symmetrically about the original "g-value" resonance in a first order approximation. Their separation is equal to the isotropic hyperfine coupling constant, K_{iso}, in units of magnetic field intensity.

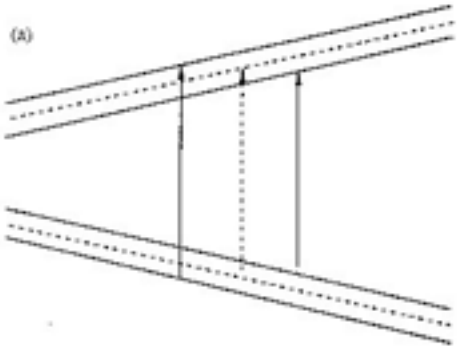

Figure 5: Energy level diagram for a paramagnet with $S = 1/2$ and $I = 1/2$.

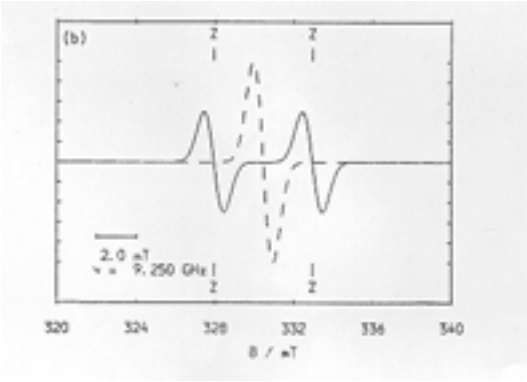

Figure 6: Isotropic epr spectrum for a paramagnet with $S = 1/2$ and $I = 1/2$ (The dashed lines represent the original resonance).

3 Mathematical means in tomography

The mathematical basis for tomographic imaging was laid down by Johann Radon. It is applied in Computed Tomography to obtain cross-sectional images of patients. This paper applies in general to tomographic reconstruction for all kinds of tomography [3].

3.1 Acquisition projection data

The projection of an object at a given angle, θ, is made up of a set of line integrals. In X-ray CT, the line integral represents the total attenuation of the beam of x-rays as it travels in a straight line through the object. As mentioned above, the resulting image is a 2D (or 3D) model of the attenuation coefficient. That is, we wish to find the image $\mu(x, y)$. The simplest and easiest way to visualise method of scanning is the system of parallel projection, as used in the first scanners. For this discussion we consider the data to be collected as a series of parallel rays, at position r, across a projection at angle θ. This is repeated for various angles. Attenuation occurs exponentially in tissue:

$$I = I_0 \exp\left(-\int \mu(x) dr\right) \tag{5}$$

where $\mu(x)$ is the attenuation coefficient at position x along the ray path. Therefore generally the total attenuation of a ray at position r, on the projection at angle θ, is given by the line integral:

Figure 7: Projection data acquisition

$$p(r,\theta) = \ln(I_0, I) = \int \mu(x,y)ds \tag{6}$$

Using the coordinate system of Figure 7, the value of r onto which the point (x, y) will be projected at angle θ is given by

$$x\cos(\theta) + y\sin(\theta) = r \tag{7}$$

So the equation above can be rewritten as:

$$p(r,\theta) = \int_{-\infty}^{\infty}\int_{-\infty}^{\infty} f(x,y)\delta(x\cos\theta + y\sin\theta - r)dxdy \tag{8}$$

where $f(x, y)$ represents $\mu(x, y)$. This function is known as the Radon transform (or sinogram) of the 2D object. The projection-slice theorem tells us that if we had an infinite number of one-dimensional projections of an object taken at an infinite number of angles, we could perfectly reconstruct the original object, $f(x, y)$. So to get $f(x, y)$ back, from the above equation means finding the inverse Radon transform. It is possible to find an explicit formula for the inverse Radon transform. However, the inverse Radon transform proves to be extremely unstable with respect to noisy data. In practice, a stabilized and discretized version of the inverse Radon transform is used, known as the filtered back projection algorithm.

3.2 Filtered Back-projection and the Fourier Slice Theorem

In order to reconstruct the images, we used what is known as the Fourier Slice Theorem. The Slice Theorem tells us that the 1D Fourier Transform of the projection function $p(r, \theta)$ is equal to the 2D Fourier Transform of the image evaluated on the line that the projection was taken on (the line that $p(0, \theta)$ was calculated from). So now that we know what the 2D Fourier Transform of the image looks like (or at least what it looks like on certain lines and then interpolate), we can simply take the 2D inverse Fourier Transform and have our original image.

We can show the Fourier Slice Theorem in the following way:

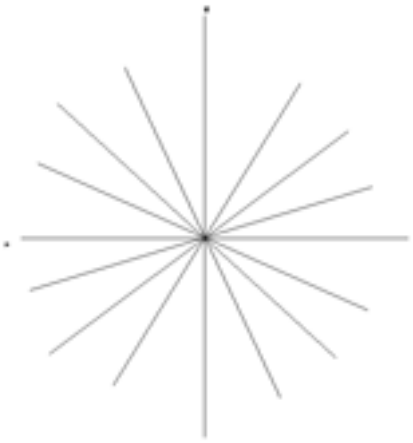

Figure 8: Arbitrary directions of projection slices

The 1D Fourier Transform of p is given by:

$$P(\omega, \theta) = \int e^{-j\omega r} p(r, \theta) dr \tag{9}$$

Now, we subsitute our expression for $p(r, \theta)$ (Eqn. 8) into the expression above to get:

$$P(\omega, \theta) = \int \int \int f(x, y) e^{-j\omega r} \delta(x \sin\theta - y \cos\theta - r) dx dy \tag{10}$$

We can use the sifting property of the Dirac delta function to simplify to:

$$P(\omega, \theta) = \int \int f(x, y) e^{-j\omega(x \sin\theta - y \cos\theta - r)} dx dy \tag{11}$$

Now, if we recall the definition of the 2D Fourier Transform of f:

$$F(u, \nu) = \int \int f(x, y) e^{-j(ux + \nu y)} dx dy \tag{12}$$

we can see that that Eqn. 11 is just $F(u, \nu)$ evaluated at $u = \omega \sin(\theta)$ and $\nu = -\omega \cos(\theta)$, which is the line that the projection $p(r, \theta)$ was taken on!

Now that we have shown the Fourier Slice Theorem, we can continue with the math to gain further insight. First, recall the definition for the 2D inverse Fourier Transform

$$f(x, y) = \frac{1}{4\pi^2} \int \int F(u, \nu) e^{j(ux + \nu y)} dx dy \tag{13}$$

Now, we make a change of variable from rectangular to polar coordinates and replace $F(u, \nu)$ with $P(\omega, \theta)$ we get:

$$f(x, y) = \frac{1}{4\pi^2} \int \int P(\omega, \theta) e^{j\omega(x \sin\theta - y \cos\theta)} |\omega| d\omega d\theta \tag{14}$$

where $|\omega|$ is the determinant of the Jacobian of the change of variable from rectangular to polar coordinates. We now have a relationship between the projection functions and the image we are trying to recontruct, so we can easily write a program to do the reconstruction.

Notice that we have to multiply our projections by $|\omega|$ in the Fourier domain. This product

$$Q(\omega, \theta) = P(\omega, \theta) |\omega| \tag{15}$$

is called the filtered back projection at angle θ. If we look at Figure 8, we can see that we have a lot of information at low frequencies (near the origin), and not as much at high frequencies. The $|\omega|$, which is a ramp filter, compensates for this.

3.3 Example

Below, we show our phantom object reconstructed from 1, 4, 8, 15, and 60 filtered back projections.

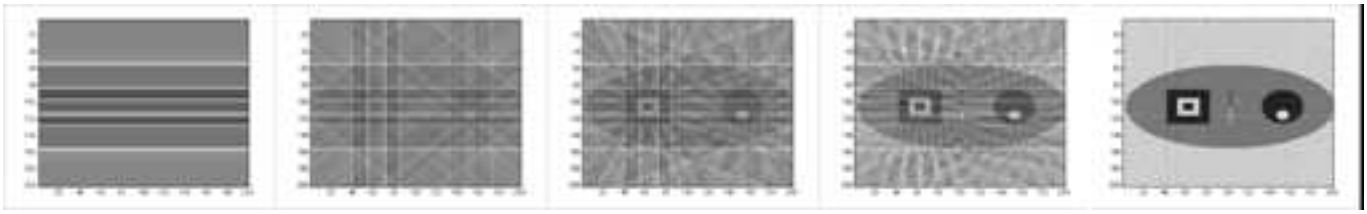

Figure 9: a) With only one back projection, not much information about the original image is revealed. b) With 4 back projections, we can see some of the basic features start to emerge. The two squares on the left side start to come in, and the main ellise looks like a diamond. c) At 8 back projections, our image is finally starting to take shape. We can see the squares and the circles well, and we can make out the basic shape of the main ellipse. d) With 15 back projections, we can see the bounds of the main ellipse very well, and the squares and cirlces are well defined. The lines in the center of the ellipse appear as blurry triangles. Also, we have a lot of undesired residuals in the back ground (outside the main ellipse).

At 60 back projections, our reconstructed image looks very nice. We still have some patterns outside the ellipse, and there are streaks from the edge of the squares all the way out to the edge of the image. These appear because the edge of the square is such a sharp transistion at 0 and 90 degrees, that when we pass the projections through the ramp filter, there are sharp spikes in the filtered projections. These never quite seem to get smoothed out.

4 EPR tomography methodology

In spite of the excitement felt by some researchers of the promise of EPR imaging, there were others who challenged the practicality, including one whose famous mantra was that "the only problem with EPR imaging is that there is nothing to image and no way to image it." Subsequent success in many labs, including the illustrations above, has shown that there is something to image and a way to image it. Thus, let's continue our introduction by discussing how an image is generated [1].

4.1 Encoding spatial information with gradient

A simple sketch of the fundamentals of an EPR imaging measurement is presented in the figure 10. In a normal CW EPR measurement a figure of merit of the EPR spectrometer is the homogeneity of the magnet. In the imaging measurement one purposefully superimposes a well-defined magnetic field gradient on the normally homogeneous magnetic field. The microwave frequency is kept constant, as in the normal EPR measurement, so that as the magnetic field (B_{ext} in the figure 10) is swept (scanned) the spins will be resonant at different values of B_{ext}.

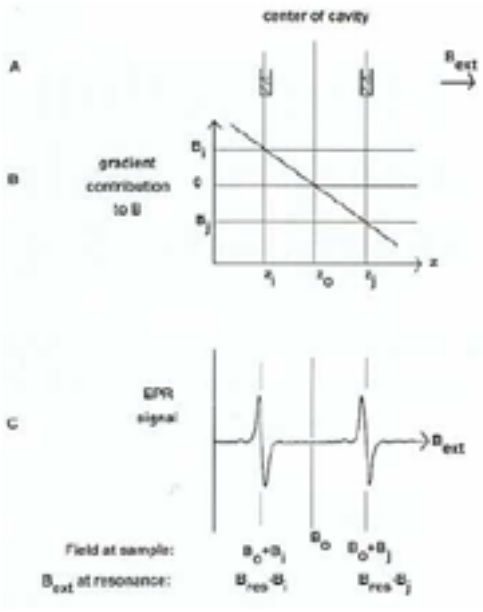

Figure 10: Precis of the EPR-imaging experiment. (A) Two samples of the same material are placed in an EPR resonator, at positions Z_i and Z_j. (B) A magnetic field gradient is applied, such that the gradient is zero at position Z_0, the gradient adds an amount B_i to the uniform, externally applied Zeeman field (B_{ext}) at position Z_i and an amount B_j at position Z_j. Because B_j is negative, the net field at Z_j is smaller than at Z_0. (C) During a CW field-swept EPR measurement, the two samples achieve resonance at different values of the slowly-swept B_{ext}.

All that is required to perform an EPR image measurement with one spatial dimension is to make any standard EPR measurement in the presence of a magnetic field gradient. The gradient could be produced by any of the methods listed below. The larger the gradient, the greater the spatial resolution of the image. Deconvolution of the spectral lineshape can be used to improve the resolution (see **??**).

Now we ask the question – how can we create an image with more than one dimension? Consider what we observe as we change the orientation of the gradient relative to our object. Note that in all of our experiments the orientation of the magnetic field is the same – along the z-axis. A gradient along the z axis means that the magnitude of B varies along the z axis, i.e we have a non-zero dB_z/dz. A gradient along the y axis means that we have nonzero dB_z/dy.

The following figure from 11 illustrates the changes in the spectra for two tubes of nitroxyl solution that occur depending on the orientation of a constant magnitude magnetic field gradient relative to the vector between the two tubes. When the gradient is along the axis between the two tubes, the maximum separation between signals is observed. Except for the complexity of the nitrogen hyperfine, which we will revisit shortly, this is the "view" that we would have if we looked at the object perpendicular to the inter-tube vector. As the orientation of the gradient changes, the separation between the two signals decreases, which corresponds to what we would "see" as we viewed the physical object from different directions.

An image is reconstructed from views of the object from many different orientations. These views are called projections and an EPR spectrum obtained at a particular gradient is called a projection. Each combination of gradients along the various axes defines a different viewing angle and the spectrum obtained at that combination of gradients is the projection of the image viewed at that angle. There are a variety of different mathematical procedures that can be used to take a set of projections and recreate an image (see 3.1, 3.2).

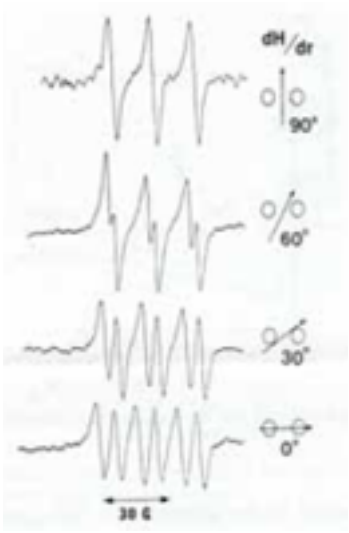

Figure 11: Two-dimensional EPR gradient projection spectra for two capillary phantom of nitroxyl solutions spaced at 3.04 mm apart. The arrows correspond to the field gradient, dH/dr (29.6 G/cm).

In the figure 7 an example is shown of a projection for a 2D object, and of the distribution of spins, obtained by a Radon transform of the projections. The mathematics is a bit complicated, and would be a diversion from this introductory overview. The key point is that we are distinguishing between spins at various locations in the sample by applying magnetic field gradients in varying directions.

Most EPR signals contain structure due to hyperfine and/or g-anisotropy. How do these characteristics of EPR spectra impact the imaging experiments? If the hyperfine splitting were uniform through the sample, as was the case for the two tubes of nitroxyl solution, the hyperfine could be removed by deconvolution. The more interesting (and more complicated) question is how to include a spectral dimension in an image.

4.2 Spectral-spatial imaging

To understand how to treat the spectral dimension consider the sketch in the figure 12, which shows the impact of a gradient on a sample that consists of one single-line spectrum and one two-line spectrum.

4.3 What to image?

Many samples of interest have inherent free radicals or paramagnetic metals, which is why EPR was used in the first place. For example, one might ask where the defects are in a sample of material irradiated with γ-rays, or a sample into which metal ions were diffused. In these cases the inherently paramagnetic species is the one whose location is sought. Alternatively, one might add a paramagnetic species as a probe of the physical phenomenon to be studied. For example, if the location of a fluid is of interest, one could add a small spin probe, such as a nitroxyl radical, which would be expected to be present wherever the fluid of interest is present, and monitor the EPR signal of the nitroxyl spin probe. Transient radicals can be monitored by using spin traps, such as nitrones.

Although many free radicals are involved in normal physiology and in pathological physiology, these usually are present at levels too low to study directly. Some, such as superoxide and hydroxyl, can be monitored with spin traps. Nitric oxide, NO, can be trapped by iron

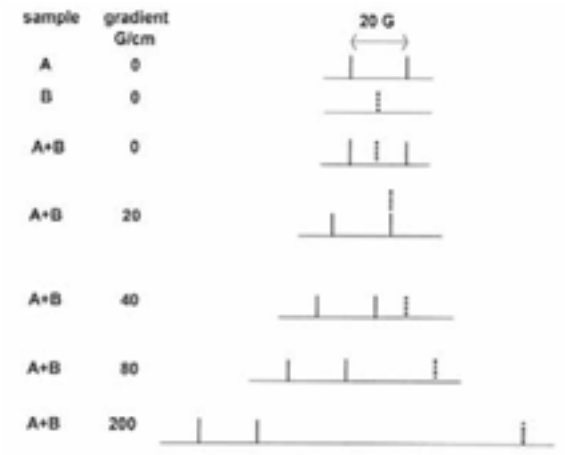

Figure 12: Stick diagram for the spectral-spatial imaging experiment. There are two, 0,5 cm apart, each is 0,25 cm from the center of the cavity. Sample A has a two-line EPR spectrum because of a hyperfine splitting of 20 G (solid sticks); sample B has a single-line EPR spectrum (dotted sticks). Because the two samples are at different spatial locations, the separation in gauss between the spectra of the two species increases as the magnetic-field gradient is increased.

dithiocarbamates and by nitronyl nitroxides, but there are also inherent NO spin traps, myoglobin and hemoglobin, which give a distinctive EPR signal. In some disease states the NO concentration may be high enough to monitor the NO trapped by myoglobin and hemoglobin without use of exogenous spin traps. Nevertheless, most in vivo EPR imaging detects free radicals introduced to the animal (or plant) as a probe. The most common probes are nitroxyl radicals, trityl radicals, and narrow-line paramagnetic solids such as lithium phthalocyanine (LiPc). By far the largest number of studies has been done with nitroxyl radicals as the EPR probe.

It has been known for a long time that carbonaceous materials exhibit EPR signals whose line width depends on the concentration of O_2. In recent years there has been renewed interest in these materials, with a focus on chars, such as from wood; carbon blacks, including the so-called India ink that is commonly used in tattoos; as well as other particulate materials such as lithium phthalocyanine (LiPc) and its derivatives, which are also sensitive probes of O_2. Although the initial placement in vivo is invasive, the subsequent monitoring by EPR is non-invasive, and time dependence can be monitored over days to weeks and months, depending on the biocompatibility of the particulate probe. These particulate probes monitor O_2 at the place where they were implanted.

In short, there are many things to image, including *in vivo*.

4.4 What information is in image?

The simplest concept of an image is the geometric, or spatial, distribution of spin concentration. This is essentially what people are familiar with from MRI, which yields such detailed pictures of anatomy. When 2D or 3D imaging is discussed, most often the meaning is 2 or 3 spatial dimensions. The intensity dimension is always implied, but never counted among the number of dimensions listed. However, the concept of multidimensional imaging is much broader than the three spatial dimensions. Almost anything that can impact an EPR spectrum can be imaged, and can conceptually constitute a dimension in an image. For example, since viscosity affects molecule tumbling and thence the EPR spectrum, one could image viscosity as a function of location in the sample, animate or inanimate.

More importantly, the goal is not just to obtain an image, but to understand a sample based upon the information in the image. This reminds us of the modern description of geography as the "why of where." We want to not only image, say, oxygen concentration in a tumor, but to understand why that concentration is what it is where it is. And, one should add, when. Time dependence of the image is important. The time dependence is central to the application of EPR imaging studying the progression of solvent diffusion in a polymer, or the measurement of diffusion or convection per se. As the needed technology is developed, *in vivo* imaging increasingly is focusing on faster measurement, not just for the sake of throughput, but to understand time-dependent changes in physiology.

4.5 Relationship between MRI and EPR Imaging

Although NMR and EPR have close conceptual similarities, the differences in the magnitudes of the nuclear and electron magnetogyric ratios, hyperfine coupling constants, and relaxation times, make the methods of performing NMR imaging and EPR imaging differ. For example, NMR imaging, almost universally called MRI, is almost always performed with spin echo detection and pulsed magnetic field gradients. EPR imaging is usually performed with CW detection and stepped static magnetic field gradients. Roughly speaking, MRI differs from EPR imaging by having about 10^5 to 10^6 higher spin concentration and about 10^5 to 10^6 longer spin relaxation times. In addition, ^{1}H NMR spectra extend over about 10 ppm (*e.g.*, 150 mG in a 15 KG (1.5 T) field), whereas many EPR spectra extend over all accessible magnetic fields, and even nitroxyl radical spectra extend over ca. 1% of the field at X-band, and about half of the field at 250 MHz. These differences make EPR imaging, whether CW or pulsed, very challenging relative to normal ^{1}H MRI.

This table summarizes parameters important to the comparison of MRI and pulsed EPR imaging.

	NMR Imaging	EPR Imaging
T_1	hundreds of ms to seconds	5.9-6.2 μs trityls; ¡ 1 μs nitroxyls
T_2	tens of ms to seconds	4.3-5.3 μs trityls; ¡0.5 μs nitroxyls
echo time	tens of ms	a few μs
gradient rise time	pulse, ca. 100 μs rise time	constant, stepped between projections
magnet and resonator orientation	usually, solenoid magnet, B_1 $\perp$ resonator axis, which is $\parallel$ to magnet axis	B_1 $\parallel$ resonator axis, which is $\perp$ to magnet axis to facilitate animal access
RF pulse power	5-23 KW peak power	l 400 W so far
magnet homogeneity	l 5 ppm	$\pm$ 40 ppm
magnetic susceptibility	effects are important so need to shim for each image	negligible; no shimming needed

The electron spin relaxation times cited in this table are those for the substituted triaryl methyl radicals called OX31 and OX63 or for nitroxyls, and the other experimental parameters are based on recent work in the labs of Murali Krishna, Howard Halpern, and the Eatons.

5 Applications

5.1 Applications to Materials Science

γ-Irradiation of UHMWPE- EPR Spectroscopic and Imaging Studies of the Mechanism of Sub-Surface Oxidation

Shelf aging of irradiated ultrahigh molecular weight polyethylene (UHMWPE) causes subsurface oxidation leading to failure in UHMWPE orthopedic components, yet the mechanisms causing subsurface oxidation remain unclear. Shelf aging of γ-irradiated UHMWPE bars was studied by spectral-spatial EPR and NMR imaging, and by microtoming and Fourier transform infrared (FTIR) microscopy. Bars initially contained solely allyl radicals. Upon air exposure, a surface layer of peroxyl radicals formed by reaction of allyl radicals with oxygen. Importantly, a band of low radical intensity just beneath the peroxyl layer became apparent. NMR imaging showed altered proton relaxation in this zone. With increasing time, surface peroxyl radicals persisted longer than the allyl radical in the interior, although oxygen did not appear to penetrate any deeper into the bar. The area of maximal oxidation and mechanical disruption, measured after 3 years, was at the interface between the zone of exterior peroxyl radical and the zone of low radical intensity. See Figure 13 [1].

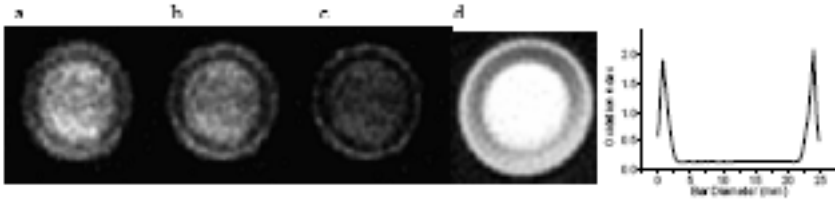

Figure 13: Subsurface UHMWPE oxidation in a sample of γ-irradiated UHMWPE after 2.5 years shelf aging. Overlays of representative 1^{st} derivative EPR images at fields a) 39.46 and b) 39.62 mT (maximizing display of subsurface zone of low radical concentration) of 100 kGy irradiated UHMWPE after 9 months shelf aging, co-registered with c) the image of maximal subsurface oxidation obtained by microtoming and d) a slice of sample after 40 months obtained by summing the NMR image over 23 planes (18.4 mm) in z. Also shown in e) is oxidation index measured as carbonyl content by FTIR of a thin microtomed section (in steps of 0.2 mm). (Figure and description provided by Graham Timmons, 2004).

5.2 Applications in Electrochemistry

It is well-known that one way to generate radicals for study by EPR is electrochemical oxidation or reduction. EPR imaging can reveal where the radical is generated, and in some cases provide insight into the mechanism of the electrochemical reactions. One of the classic experiments is to generate a semiquinone radical from either the quinine or the hydroquinone. How does this happen in an electrochemical EPR cell? When reduction of p-benzoquinone occurred at the Pt working electrode (figure 14 left-hand image) there was line broadening near the electrode due to rapid electron transfer between the semiquinone radical produced and the bulk concentration of quinone. When the same radical was formed by oxidation of the hydroquinone, there was actually a two-step mechanism in which quinone was produced from the hydroquinone at the working electrode, and the quinone then diffused to the auxiliary electrode where it was reduced to the semiquinone observed by EPR (figure 14 righthand image) [1].

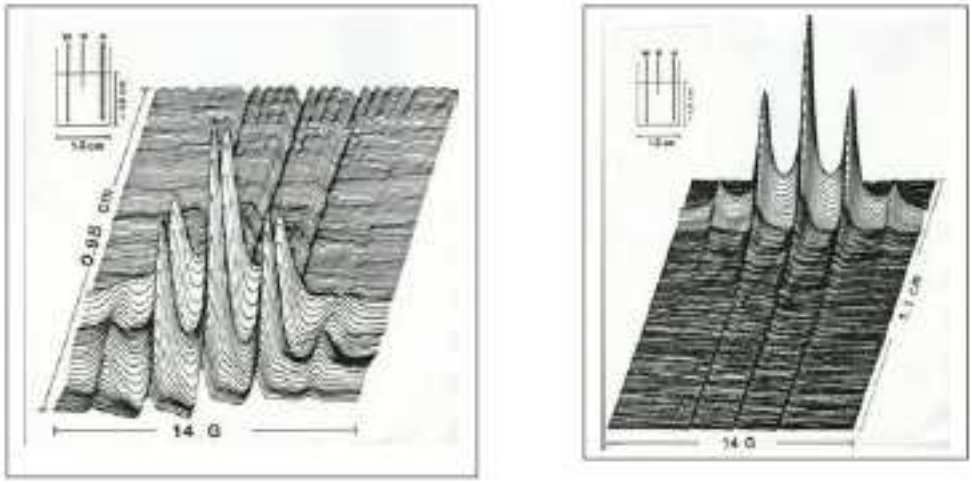

Figure 14: Applications in Electrochemistry

5.3 Applications to Diffusion

Freed and coworkers have measured diffusion coefficients of nitroxyl radicals in several solvents, including liquid crystals. They were able to measure both microscopic and macroscopic diffusion for the same probe in the same sample under the same conditions, and show that Dmicro is substantially greater than Dmacro [1].

5.4 Application to Biological Systems - Animals

Very large objects can be imaged without placing them "inside" a resonator. For example a human may not fit into resonators at microwave frequencies, but much can be learned about the physiology of the skin of a human being by using a surface coil. Herrling and coworkers measured the kinetics of reduction of a nitroxyl radical on the skin of a human forearm with an S-band (2.4 GHz) 4 mm diameter surface coil. A half life of 4.8 minutes was found (Herrling *et al.*, 2002). However, was this due to reduction in the skin or transport away from the resonator? 2D images showed that there was no significant change in positional distribution in 2 hours, so the temporal changes in intensity were due to bioreduction [1].

The next question, then, is which skin layers are involved. By imaging the central line of a nitroxyl with a magnetic field gradient perpendicular to the skin, and repeating images as a function of time, it was shown that the nitroxyl was mostly in the upper skin layers.

In contrast to these S-band studies, ex vivo studies (6 mm diameter skin biopsies) could be performed at X-band.

5.5 Rat's heart ischemia-reperfusion

The Zweier lab explores ischemia and reperfusion injury of the heart, with EPR imaging as an important tool. The following figure, selected from a large body of work, illustrates the correspondence between EPR imaging and histology (Velayutham *et al.*, 2003), figure 16 [1]:

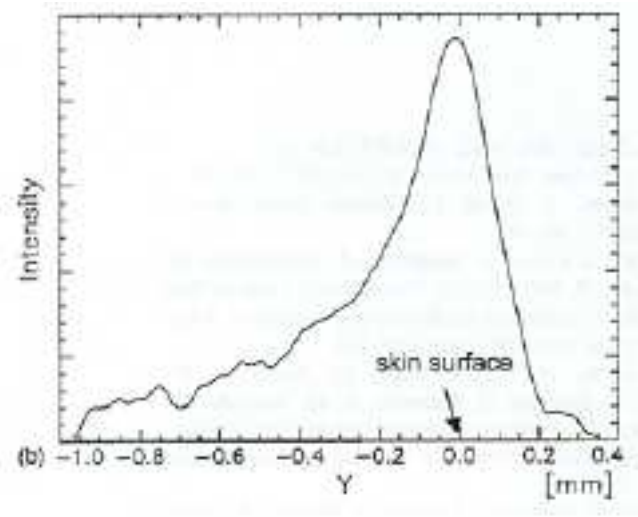

Figure 15: Skin Image

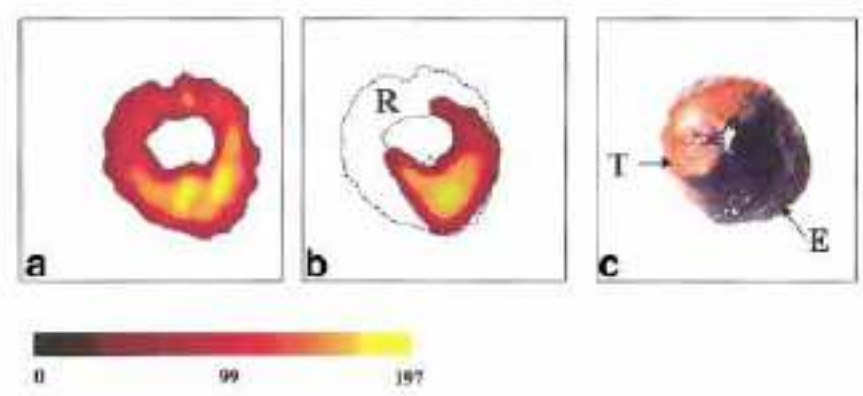

Figure 16: Comparison of EPRI and histology for measurement of myocardial risk region. a,b: Slices from the 3D spatial EPRI of control and LAD occluded hearts respectively. c: Image of a corresponding central heart slice. The heart was perfused with cardioplegic buffer containing 1,5 mM 3-CP and regional ischemia was created by LAD occlusion. At the end of the EPR measurements the hearts were removed and the risk region assessed using Evans blue dye. The infarct size was measured by TTC staining. In c, the Evans blue colored no-risk region and red TTC colored risk region, denoted by E and T, respectively. The void in intensity at the anterior region, R, in slice b corresponds closely with the position and size of the red-colored risk region, T, seen on histology in slice c.

References

[1] 27th International EPR Symposium "EPR Imaging Workshop", August 1, 2004, Denver.

[2] Manchester University Department of Chemistry,
http://mch3w.ch.man.ac.uk/services/epresr/EPRprcip2.htm

[3] Free Encyclopedia,
http://www.wikipedia.org/